Asian Journal of Physical and Chemical Sciences

Volume 10, Issue 4, Page 41-68, 2022; Article no.AJOPACS.95772
ISSN: 2456-7779

Contribution of the Provençal Well for the Improvement of the Thermal Comfort in the Building in Turbulent Regime

Kokou N'wuitcha [a*], Ouro-Djobo Essoavana Samah [b], Yendouban Kolani [a], Magolmèèna Banna [a] and Belkacem Zeghmati [c]

[a] Department of Physics, Solar Energy Laboratory, University of Lome, P.O. Box 1515, Lome, Togo.
[b] Regional Training Centre for Road Maintenance (CERFER) – 1704, Bd de la paix 01, P.O Box: 1369 Lome, Togo.
[c] Department of Physics, Laboratory of Mathematics and Physics, University of Perpignan, 52 Avenue Paul Alduy, 66860 Perpignan Cedex, France.

Authors' contributions

This work was carried out in collaboration among all authors. All authors read and approved the final manuscript.

Article Information

DOI: 10.9734/AJOPACS/2022/v10i4189

Open Peer Review History:
This journal follows the Advanced Open Peer Review policy. Identity of the Reviewers, Editor(s) and additional Reviewers, peer review comments, different versions of the manuscript, comments of the editors, etc are available here: https://www.sdiarticle5.com/review-history/95772

Original Research Article

Received: 27/10/2022
Accepted: 30/12/2022
Published: 31/12/2022

ABSTRACT

In the current energy context, geothermal systems are highly developed in the building field. Among these interesting systems on the energy plan, one finds in particular the earth-to-air heat exchanger commonly called 'Canadian or Provençal well'. It consists of tubes buried in which the ambient air is pushed in order to be refreshed in contact with the ground whose temperature is quasi-constant throughout the year. In this work, a study of the performance of an earth-to-air heat exchanger was undertaken by means of numerical modeling of heat exchange by forced

**Corresponding author: E-mail: knwuitcha@gmail.com;*

convection in a buried tube. The transfer equations in the tube are discretized using the finite volume method in turbulent regime and solved using the Thomas algorithm. For the determination of the ground temperature, the model of the semi-infinite mass subjected to a periodic excitation was adopted. The soil temperature was used as a boundary condition for the buried tube.
The results show that the interest of the earth-to-air heat exchanger is major, since it improves throughout the year, the thermal conditions sought. It intervenes in an effective way on the damping of the thermal amplitudes in the building. The variation of the diameter and the length of earth-to-air heat exchanger does not influence notably the distribution of the streamlines and isotherms but affect significantly the values of stream function and temperature inside de tube of the earth-to-air heat exchanger. When diameter of the pipe increases, the outlet temperature increases. The increase of the length of the earth-to-air heat exchanger leads to the isotherms increase as a result of the intensification of heat exchange between the walls and the convective jet. The temperature in the air outlet compartment is lower as the length of the earth-to-air exchanger increases.

Keywords: Earth-to-air heat exchanger; canadian well; geothermal energy; building air conditioning; heat transfer.

NOMENCLATURE

Symbol Description

D : diameter of the buried tube (m)
g : Gravity (m/s²)
H : depth of the earth-to-air heat exchanger (m)
k : Average turbulent kinetic energy (m²/s²)
L : length of horizontal part of buried tube (m)
p : Average pressure (Pa)
P_r *: Prandtl number*
t : Dimensional time (s)
T_0 *: Reference temperature (K)*
T_{min} *: minimum average temperature of the year* (K)
T_{max} *: maximum average temperature of the year* (K)
T_{soil} *: soil temperature* (K)
u : dimensional velocity component in x-direction $(m.s^{-1})$
v : dimensional velocity component in y-direction $(m.s^{-1})$
V_0 *: inlet velocity* $(m.s^{-1})$
x *: cartesian coordinate in horizontal direction (m)*
y *: cartesian coordinate in vertical direction (m)*

Greek Symbols

α_{soil} *: soil thermal diffusivity* $(m^2.s^{-1})$
θ : Average dimensional air temperature in the tube (K)
ω *: Pulsation* $(rad.s^{-1})$
ε : Average turbulent kinetic energy dissipation
ν *: Kinematic viscosity (m²/s)*
ν_t *: Turbulent kinematic viscosity (m²/s)*
μ *: Dynamic viscosity* $\left(k_g.m^{-1}.s^{-1}\right)$
μ_t *: Dynamic turbulent viscosity* $\left(k_g.m^{-1}.s^{-1}\right)$
σ_k *: Turbulent Prandtl numbers for diffusion of k*
σ_ε *: Turbulent Prandtl numbers for diffusion of ε*
ρ *: density* $(kg.m^{-3})$

Subscripts

0 : Reference
in : inlet
min : minimum
max : maximum
soil : relative to the soil
T : thermal

1. INTRODUCTION

The world has been dependent on fossil fuels for several decades due to its life style. In order to reduce this dependence, it is essential to turn to renewable energy as geothermal energy. In recent years, special attention has been paid to this technology. It is used for space heating and cooling purposes [1,2]. This kind of energy is, at principle, inexhaustible and can be found and exploited equally well on the planet [3]. The various applications of geothermal energy are geothermal electricity, ground source heat pump, earth-to-air heat exchanger...Among these applications, earth-to-air heat exchanger has the advantages of simple system, easy implementation and less expensive low operation cost [4]. This nonconventional energy source is better option of clean and sustainable energy [5].

The earth-to-air heat exchanger presented an impressive evolution during the last three decades, enriched with new research, techniques and materials. It can provide minimization of heating/cooling loads, excellent thermal comfort conditions, mitigation of the urban heat island and an amelioration of the urban environment [6-8]. Many researches have been devoted to the earth-to-air heat exchanger in order to determinate its performance [9-13]. There are several parameters that influence the performances of the earth-to-air heat exchanger: they are both geometric factors of the system and the thermo-physical parameters of the soil and air.

Selamat et al. [14] researched, through numerical modelling, the best configuration for an EAHX during winter in the city of Dublin (Ireland). The results show that an increase in the length of the tube, a decrease in the diameter of the tube and a decrease in the air velocity provide an improvement of the system heating capacity. Sodha et al. [15] made a comparison between single-tube and multiple-tube exchangers. It has been observed that, with the same air flow, the heating and cooling potential increases as the number of tubes of smaller diameter increase, because of the consequent augmentation of the heat exchange area. With the increase in pipe diameter, the absolute value of temperature variation reduces, reducing the heating/cooling capacity of the system.

Several works are conducted experimentally [16-18] in recent years on flows and heat transfers in earth-to-air heat exchanger. Such works are of particular interest in the heating and cooling of premises. Mathur et al. [19] introduced an experimental study where an earth to air spiral heat exchanger was designed with a 60-m pipe length, a diameter of 0.1 m, and a 1-m distance among the spirals, and it was buried at a depth of 3 m. The results obtained were compared to straight tube EAHX-system results: they noted that the coefficient of performance of the latter configuration is 5.94 in the cooling phase and 1.92 in the heating phase, whereas for a spiral configuration these values are 6.24 and 2.11, respectively. As Benrachi et al. reported [20], the use of the spiral configuration can be an interesting alternative to straight tube exchangers if the space available for excavation is limited. This advantage in terms of occupied area tends to disappear when dealing with the installation of several pipes in parallel.

In recent decades, a lot of research has been carried out to develop analytical and numerical models to analyse earth-to-air heat exchanger systems. The performance analysis of EAHE involves the calculation of conductive heat transfer from the pipe to the groundmass, or the calculation of convective heat transfer from the circulating air to the pipe and changes in the air temperature and humidity. Nowadays, a lot of researchers have used computational fluid dynamics (CFD) to model and study the performance analysis of the EAHE systems. This is because CFD employs a very simple rule of discretization of the whole system in small grids and governing equations applied on these discrete elements, which are done to obtain numerical solutions concerning flow parameters, pressure distribution, and temperature gradients in less time and at reasonable cost because of reduced required experimental work [21,22]. A lot of research papers on different design methods of EAHE systems have been published. Previous research conducted on the calculation models of EAHE systems are presented in the subsequent three subsections; namely, one-dimensional models [23,24], two-dimensional models [25,26], and three-dimensional models of EAHE systems [27,28].

Cucumo et al. [29] have proposed a transient one-dimensional analytical model which can be used for the correct installation and the calculation of the performances of EAHEs buried at different depths. With acceptable theory, the model is able to calculate the length and humidity ratio at the outlet section of a buried pipe at different depths of installation and to evaluate the

performance of a buried pipe of assigned length. The model was obtained by the solution of heat and mass balances for air through the buried pipe, considering a suitable temperature profile in the ground. This was achieved by two methods: the first is based on Green's functions and the second, simplified, was based on the principle of superposition. The numerical and the experimental data showed a very satisfactory agreement with each other.

A one-dimensional numerical model has been proposed by Sehli et al. [30] to check the performance of EAHEs installed at different depths. Parametric study on the effects of Reynolds number, installation depth, and form factor on the performance of an earth-to air heat exchanger (ETHE) system were analyzed. Ratio of pipe length to pipe diameter of the EAHE systems was defined as a form factor. From the result, it is found that as the installation depth increases, the form factor of the outlet air temperature decreases, while the increase in Reynolds number also causes the outlet air temperature to increase. The study finds that EAHE systems alone are not sufficient to create thermal comfort, but it can be used to reduce the energy demand in buildings in south Algeria, if used in combination with conventional air-conditioning systems.

Tittelein et al. [26] proposes a new numerical model of earth-to-air heat exchangers. The discretized model was solved using the response factors method in order to reduce computational time. Each response factor was calculated using a finite elements program which solves two-dimensional (2D) conduction problems. Based on the result, there are a few advantages of the new model, firstly the calculation time was reduced by the use of response factor. Moreover, it was precise for a short solicitation period (1-day) and a long solicitation period (1-year). Secondly, every type of soil characteristic (inhomogeneous, anisotropic etc.) and of geometry can be considered due to the response factor calculation in a 2D finite elements program (not as analytical models). Lastly, multiple pipes exchangers could be considered with their interaction by calculating more response factors. To conclude, 2D models allow calculation of soil temperature at the surface and at different depths. The finite element programs are used in 2D models to solve two-dimensional conduction problems of EAHE systems by using finite element programs.

Flaga-Maryanczyka et al. [28] have demonstrated the experimental measurements and numerical simulation of a ground source heat exchanger operating at a cold weather for a passive house ventilation system. The study carried out for a passive house was located in the South of Poland. The house and its components were fitted with a data acquisition system that was running from 2011 and records 139 points at an interval of 1 minute. The calculations were performed using the CFD ANSYS FLUENT software package. Based on the experimental data on the CFD (Computational Fluid dynamics) simulations done for the ground source heat exchanger that was operating for the passive house ventilation system on February, it showed a good correlation with the measured values. Moreover, the difference between measured and calculated values at the level of 1.7°C on average leads. Therefore, it was concluded that CFD tool is acceptable to be used for simulations of the ground source heat exchanger working in cold climates for the passive house ventilation system.

Most simulations focus on only very limited configurations based on simple one-dimensional models that can hardly predict the real behavior of an earth-to-air heat exchanger. There are little works in literature taking into accompt the air flow regime. The objective of this paper is to present a more accurate and validated, transient, implicit numerical model based on coupled and simultaneous transfer of heat and mass into the soil and the pipe. It is analyzed the parameters that would optimize the thermal performances of earth-to-air heat exchanger. The model studied takes into consideration the geographical and climatic conditions and the turbulent flow regime of air in a buried pipe.

A mathematical model is based on the conservation equations of momentum, heat to which we associated a k-ε closure model of turbulence. The ground temperature is determined analytically and used as boundary conditions for the walls of the pipe. The set of equations and boundary conditions were discretized using the finite volume method and solved by the THOMA algorithm. The results are presented in the form of streamlines and isotherms. The influence of the operating parameters (diameter, length) on the distribution of the temperature and velocity fields has been studied.

2. PROBLEM FORMULATION

2.1 Problem Configuration and Assumptions

The geometry of the considered problem is a buried pipe at a depth H in which the air flows.

This duct has a length L and an internal diameter D. The air enters the duct through the left opening with an ambient temperature Ta and a velocity U_0. The geometry of the system is shown in Fig. 1. It is designate by compartment 1, the left vertical part of the earth-to-air heat exchanger where the air enters; compartment 2, the horizontal part of the earth-to-air heat exchanger and compartment 3, the right vertical part leading to the earth-to-air heat exchanger outlet.

2.2 Heat Transfer Equation in the Soil

In the study of the earth-to-air heat exchanger we will consider the soil as a semi-infinite medium. In this condition, the heat equation is written as:

$$\frac{\partial T_{soil}}{\partial t} = \alpha_{soil} \frac{\partial^2 T_{soil}}{\partial z^2} \quad \text{(A)}$$

$$T_{soil}(0,t) = T_0 + A_T Cos\,[\omega(t - t_0)] \quad \text{(B)}$$

$$T_{soil}(\infty, t) = T_0 \quad \text{(C)}$$

Where $T_0 = \frac{T_{min}+T_{max}}{2}$ and $A_T = \frac{T_{max}-T_{min}}{2}$ (D)

The analytical solution of this equation gives:

$$T_{Soil}(z,t) = T_0 + A_T exp\left(-z\sqrt{\frac{\omega}{2\alpha_{soil}}}\right).F(t,z) \quad \text{(E)}$$

With: $F(t,z) = cos\left(\omega(t - t_0) - z\sqrt{\frac{\omega}{2\alpha_{soil}}}\right)$ (F)

$$z = H - y. \quad \text{(G)}$$

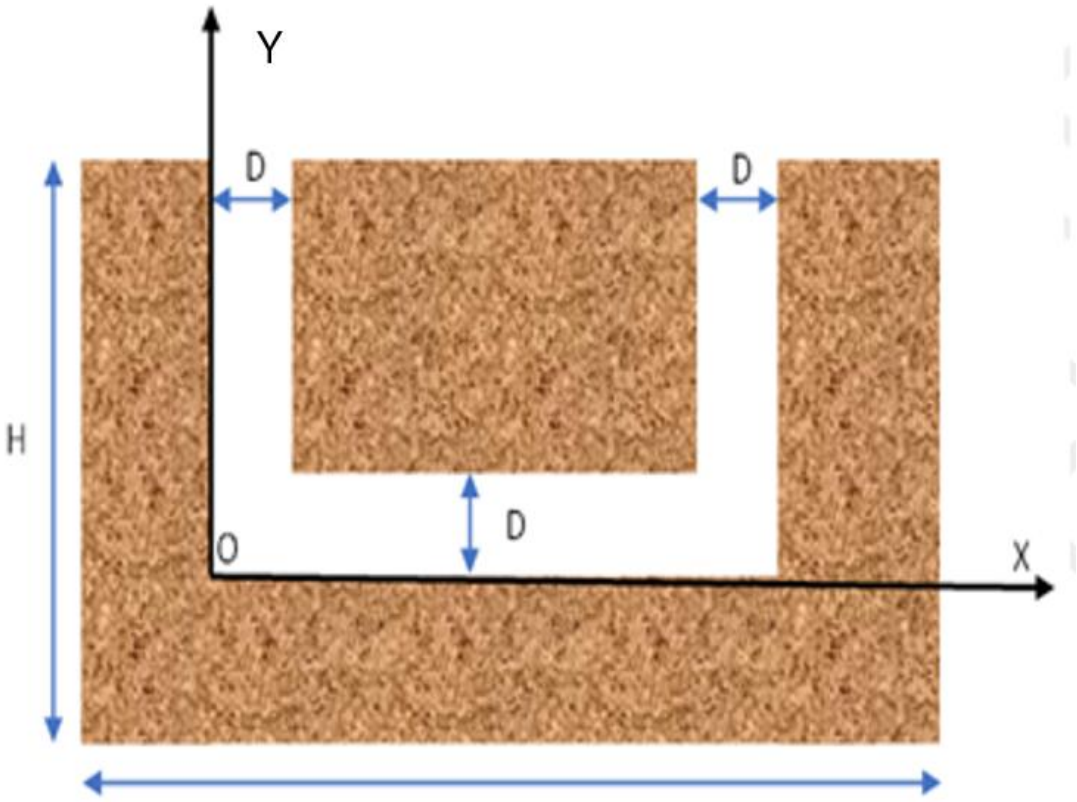

Fig. 1. Diagram of earth-to-air heat exchanger

2.3 Transfer Equations within the Earth-to-air Heat Exchanger

The study of fluid flow is approached establishing simplifying assumptions. It is assumed that:

- the flow is unsteady and turbulent.
- the flow is considered two-dimensional.
- the fluid is newtonian, and incompressible.
- there are no heat sources in the earth-to-air heat exchanger.
- radiant heat transfer is negligible.
- heat dissipation by viscous friction is neglected.
- the Boussinesq approximation is considered.

2.4 Conservative Equations

The basic equations governing the flow and heat transfer are given as follows:

- Continuity equation:

$$\frac{\partial u}{\partial x}+\frac{\partial v}{\partial y}=0 \tag{1}$$

- Momentum equation in x direction

$$\frac{\partial u}{\partial t}+\frac{\partial}{\partial x}(uu)+\frac{\partial}{\partial y}(vu)=-\frac{1}{\rho_0}\frac{\partial}{\partial x}\left(p+\frac{2}{3}\rho_0 k\right)+\frac{\partial}{\partial x}\left[2(\nu+\nu_t)\left(\frac{\partial u}{\partial x}\right)\right] +\frac{\partial}{\partial y}\left[(\nu+\nu_t)\left(\frac{\partial u}{\partial y}+\frac{\partial v}{\partial x}\right)\right] \tag{2}$$

- Momentum equation in y direction

$$\frac{\partial v}{\partial t}+\frac{\partial}{\partial x}(uv)+\frac{\partial}{\partial y}(vv)=-\frac{1}{\rho_0}\frac{\partial}{\partial y}\left(p+\frac{2}{3}\rho_0 k\right)+\frac{\partial}{\partial x}\left[(\nu+\nu_t)\left(\frac{\partial u}{\partial y}+\frac{\partial v}{\partial x}\right)\right] +\frac{\partial}{\partial y}\left[2(\nu+\nu_t)\left(\frac{\partial v}{\partial x}\right)\right]+\rho g\beta\left(\theta-\theta_0\right) \tag{3}$$

- Energy equation

$$\frac{\partial \theta}{\partial t}+\frac{\partial}{\partial x}(u\theta)+\frac{\partial}{\partial y}(v\theta)=\frac{\partial}{\partial x}\left[\left(\frac{\nu}{\mathrm{Pr}}+\frac{\nu_t}{\sigma_t}\right)\frac{\partial \theta}{\partial x}\right]+\frac{\partial}{\partial y}\left[\left(\frac{\nu}{\mathrm{Pr}}+\frac{\nu_t}{\sigma_t}\right)\frac{\partial \theta}{\partial y}\right] \tag{4}$$

These equations are completed by the equations of the $k-\varepsilon$ standard model:

- Turbulent kinetic energy transport equation

$$\frac{\partial k}{\partial t}+\frac{\partial}{\partial x}(uk)+\frac{\partial}{\partial y}(vk)=\frac{\partial}{\partial x}\left[\left(\nu+\frac{\nu_t}{\sigma_k}\right)\frac{\partial k}{\partial x}\right]+\frac{\partial}{\partial y}\left[\left(\nu+\frac{\nu_t}{\sigma_k}\right)\frac{\partial k}{\partial y}\right]+P_k+G_k-\varepsilon^* \tag{5}$$

- Dissipation of turbulent kinetic energy transport equation

$$\frac{\partial \varepsilon^*}{\partial t}+\frac{\partial}{\partial x}(u\varepsilon^*)+\frac{\partial}{\partial y}(v\varepsilon^*)=\frac{\partial}{\partial x}\left[\left(\nu+\frac{\nu_t}{\sigma_\varepsilon}\right)\frac{\partial \varepsilon^*}{\partial x}\right]+\frac{\partial}{\partial y}\left[\left(\nu+\frac{\nu_t}{\sigma_\varepsilon}\right)\frac{\partial \varepsilon^*}{\partial y}\right] +C_1 f_1 \frac{\varepsilon^*}{k}\left(P_k+C_3 G_k\right)-C_2 f_2 \frac{\varepsilon^{*2}}{k} \tag{6}$$

With :

$$\begin{cases} P_k = 2\nu_t\left[\left(\frac{\partial u}{\partial x}\right)+\left(\frac{\partial v}{\partial y}\right)\right]+\nu_t\left[\left(\frac{\partial v}{\partial x}\right)+\left(\frac{\partial u}{\partial y}\right)\right] \\ G_k = -g\beta\frac{\nu_t}{\sigma_t}\left(\frac{\partial \theta}{\partial y}\right) \end{cases} \tag{7}$$

$$\nu_t = C_\mu f_\mu \frac{k^2}{\varepsilon}\ ;\quad f_\mu = \exp\left(\frac{-3.4}{\left(1+\frac{\mathrm{Re}_T}{50}\right)^2}\right)\ ;\ \mathrm{f}_1 = 1\ ;\quad f_2 = 1-0.3\exp\left(-\mathrm{Re}_T{}^2\right) \tag{8}$$

The constants of the turbulent model are defined as in Table 1.

Table 1. Values of the constants of the turbulence model

C_μ	σ_t	σ_k	σ_ϵ	C_1	C_2	C_3
0.09	1	1	1.3	1.44	1.92	0.70

2.5 Initial and Boundary Conditions

2.5.1 Initial conditions

The initial conditions used to solve the transfer equations are as follows:

For t = 0, $u = 0$; $v = 0$; $T = T_0$; $k = 10^{-3}$; $\varepsilon^* = 10^{-3}$ (9)

2.5.2 Boundary conditions

To solve the equations that govern the phenomenon studied, we associated the following boundary conditions:

- At the entrance of the earth-to-air heat exchanger: $0 \le x \le D$, $y = H$

$$u = 0\ ; = -V_0\ ;\ T = T_0\ ; k = k_{in} = 0.005v_0^2\ ,\ \varepsilon = 0.01k_{in}^2\ ;\ P = P_0 \tag{10}$$

- At the exit of the earth-to-air heat exchanger: $L - D \le x \le L$, $y = H$

$$\left.\frac{\partial \mathrm{u}}{\partial y}\right|_{y=H} = 0\ ;\left.\frac{\partial \mathrm{v}}{\partial y}\right|_{y=H} = 0\ ;\left.\frac{\partial \mathrm{T}}{\partial y}\right|_{y=H} = 0\ ;\left.\frac{\partial \mathrm{k}}{\partial y}\right|_{y=H} = 0\ ;\left.\frac{\partial \varepsilon}{\partial y}\right|_{y=H} = 0\ ;\left.\frac{\partial \mathrm{P}}{\partial y}\right|_{y=H} = 0 \tag{11}$$

- At left vertical side of compartment 1: $x = 0$; $0 \le y \le H$

$$u = v = 0\ ; = T_{soil}\ ; k = 0\ ; \varepsilon^* = 0\ ;\left.\frac{\partial \mathrm{P}}{\partial x}\right|_{x=0} = 0 \tag{12}$$

- At right vertical side of compartment 1: $x = D$; $D \leq y \leq H$

$$u = v = 0 \; ; = T_{soil} \; ; \; k = 0 \; ; \; \varepsilon^* = 0 \; ; \; \frac{\partial \mathrm{P}}{\partial x}\Big|_{x=D} = 0 \tag{13}$$

- At lower horizontal sides of compartment 2 : $0 \leq x \leq L$, $y = 0$

$$u = v = 0 \; ; = T_{soil} \; ; \; k = 0 \; ; \; \varepsilon^* = 0 \; ; \; \frac{\partial \mathrm{P}}{\partial y}\Big|_{y=0} = 0 \tag{14}$$

- At upper horizontal sides of the compartment 2 : $D \leq x \leq L - D$, $y = D$

$$u = v = 0 \; ; = T_{soil} \; ; \; k = 0 \; ; \; \varepsilon^* = 0 \; ; \; \frac{\partial \mathrm{P}}{\partial y}\Big|_{y=D} = 0 \tag{15}$$

- At Left vertical side of compartment 3 : $x = L - D$; $D \leq y \leq H$

$$u = v = 0 \; ; = T_{soil} \; ; \; k = 0 \; ; \; \varepsilon^* = 0 \; ; \; \frac{\partial \mathrm{P}}{\partial x}\Big|_{x=L-D} = 0 \tag{16}$$

- At right vertical side of compartment 3: $x = L$; $0 \leq y \leq H$

$$u = v = 0 \; ; = T_{soil} \; ; \; k = 0 \; ; \; \varepsilon^* = 0 \; ; \; \frac{\partial \mathrm{P}}{\partial x}\Big|_{x=L} = 0 \tag{17}$$

3. NUMERICAL METHODOLOGY

3.1 Discretization of Transport Equation

The general transport equation in a two-dimensional incompressible flow is written in the Cartesian system as follows:

$$\frac{\partial \phi}{\partial t} + \frac{\partial}{\partial x_j}\left(u_j \phi\right) = \frac{\partial}{\partial x_j}\left(\Gamma \frac{\partial \phi}{\partial x_j}\right) + S_\phi \tag{18}$$

With $j \epsilon \{1; 2\}$ (index of summation)

$\frac{\partial \phi}{\partial t}$: Transient term that represents the accumulation of the variable Φ over time.

$\frac{\partial}{\partial x_j}\left(u_j \phi\right)$: transport of Φ by convection, $\frac{\partial}{\partial x_j}\left(\Gamma \frac{\partial \phi}{\partial x_j}\right)$: diffusion transport of Φ, Γ : diffusion coefficient, S_ϕ: source term.

The general form of the discretized algebraic equation using finite volume method [31] is as follows:

$$a_P \phi_P = a_E \phi_E + a_W \phi_W + a_N \phi_N + a_S \phi_S + b \tag{19}$$

The source term is discretized using a finite volume method and then linearized as a function of variable ϕ at node P.

$$\overline{S_\phi} = S_c + S_P \phi_P \tag{20}$$

The algebraic equations obtained previously can be written in the following general form:

$$A(I,J)\phi(I,J-1) + B(I,J)\phi(I,J) + C(I,J)\phi(I,J+1) = D(J) \tag{21}$$

The resulting system of algebraic equations is a tridiagonal system of algebraic equations solved using the Thomas algorithm [32] associated with an iterative procedure with a sub-relaxation coefficient equal to 0.5 for the velocity components and 0.8 for the temperature, turbulent kinetic energy, energy dissipation rate and pressure.

In order to satisfy the principle of conservation of mass and energy at each time step, the following convergence criterion must be verified for each variable :

$$\frac{Max\left(|\phi(I,J)^{k+1}-\phi(I,J)^{k}|\right)}{|\phi^{k}(I,J)|} \leq \epsilon \tag{22}$$

Where k represents the number of iterations and ϵ the precision taken at 10^{-4}.

3.2 Validation of Numerical Code

To validate our calculation code, the numerical results obtained are compared with the experimental results obtained by Ampofo et al. [33] and the numerical results of Henkes et al. [34]. Fig. 2 presents the comparison of vertical velocity and the temperature along the vertical centerline obtained by our numerical work and the experimental results of Ampofo et al. [33]. It is observed that our results are in good agreement with those of Ampofo et al. [33]. It is also qualitatively compared the flow structure (Fig. 3), the isotherms (Fig. 4) and the turbulent viscosity contours (Fig. 5) from the present work and those of Henkes [34]. As it can be seen in these figures, there is a good agreement between the results obtained in the present study and those of Henkes [34].

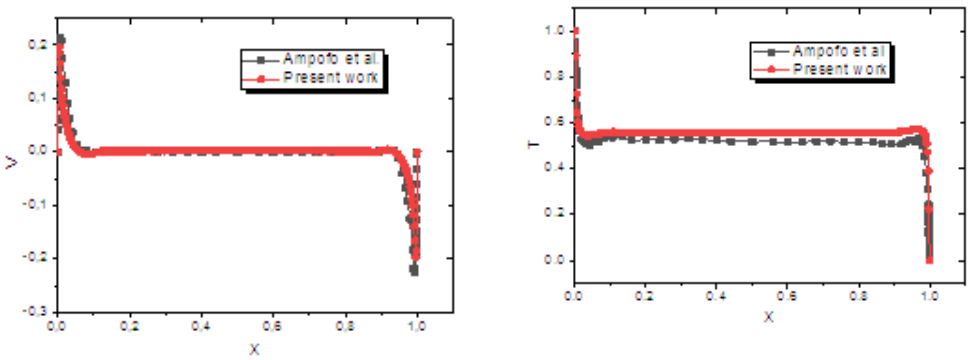

(a) **(b)**

Fig. 2. Comparison of vertical velocity (a) and temperature (b) profiles versus x at y = 0.5

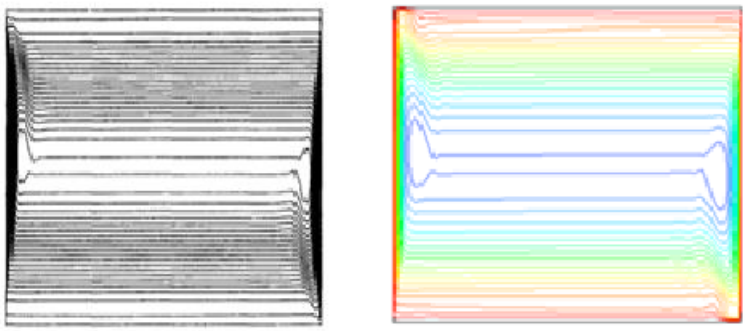

(a) Henkes et al. [34] **(b) Present work**

Fig. 3. Comparison of streamlines

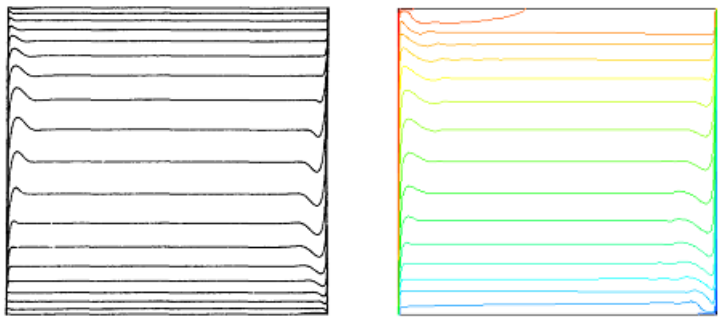

(a) Henkes et al. [34] **(b) Present work**

Fig. 4. Comparison of isotherms

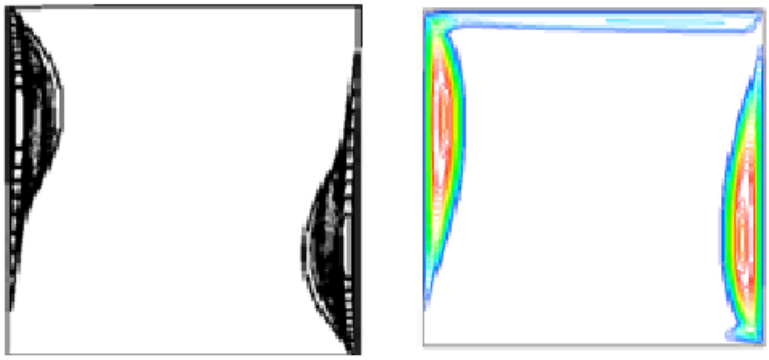

(a) Henkes et al. [34] **(b) Present work**

Fig. 5. Comparison of isotherms

4. RESULTS AND DICUSSION

4.1 Flow Structure and Isotherms

Fig. 6 shows the distribution of the streamlines and isotherms for a Reynolds number of 10000. In compartments 1, 2 and 3 of the earth-to-air heat exchanger, the streamlines (Fig. 6.a) are almost parallel to each other and to the channel walls. The streamlines laminate the walls except in the lower corners of the channel where there is a separation of the flow. The analysis of the stream function values shows that the highest values are observed at the right wall of compartment 1, the top wall of compartment 2 and the left wall of compartment 3. However, low values of the stream function are observed in the vicinity of the other walls of the exchanger.

The examination of Fig. 6.b shows that isotherms present the parabolic shaped cells originate at the inlet of the earth-to-air heat exchanger and present their peaks in the core of the main flow evolving from compartment 1 to compartment 2 and from the latter to the outlet of compartment 3. The different isotherms with increasing size as they progress through the earth-to-air heat exchanger are superimposed on each other and follow the shape of the tube. Near the walls, these isotherms become narrower, indicating the existence of intense exchanges of heat by convection and conduction between the air and the walls of the tube, especially in compartments 1 and 2. This distribution results from the fact that the temperature of the ambient air jet in the earth-to-air heat exchanger is higher than the temperature of the ground in thermal equilibrium with the tube of earth-to-air heat exchanger. It can be seen that, in accordance with the flow structure, the isotherm distribution is dense in the first half of the exchanger showing that convective transfers are preponderant there. In compartment 3, the temperature distribution is almost homogeneous due to the slowing down of the convective transfers due to the rise of the cooled air towards the exchanger outlet. Indeed, the analysis of the temperature values in the earth-to-air heat exchanger shows that the temperatures decrease progressively from the

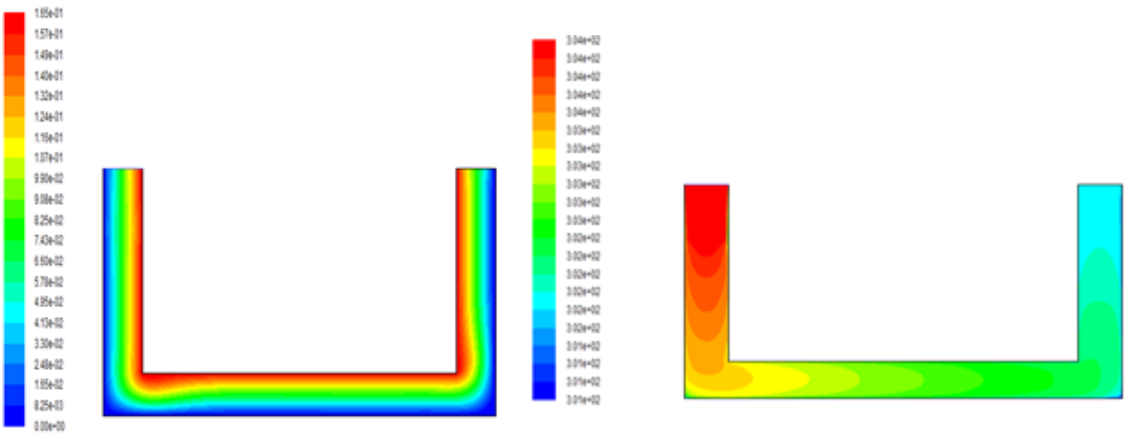

(a) Streamlines **(b) Isotherms**

Fig. 6. Streamlines and isotherms distribution for Re=10000

inlet to the outlet of the earth-to-air heat exchanger. This result is explained by the fact that air during its stay in the exchanger cools down, as the temperature of the ground being lower than that of the ambient air.

4.2 Turbulence Characteristic Parameters

The turbulent kinetic energy distribution is shown in Fig. 7.a. It represents the kinetic energy of the velocity fluctuations. It can be seen that it is more important in the vicinity of the lower corners of the earth-to-air heat exchanger where the fluid starts to turn. Indeed, the presence of singular points of pressure drop in the configuration of the earth-to-air heat changer under study (in the U-shape) causes greater fluctuations in velocity at these points and consequently an increase in the turbulent kinetic energy. The velocity fluctuations continue in the middle of the main flow in the vertical outlet branch. This observation is explained by the increase in velocities due to the combined effects of natural and forced convection in the vertical direction, which induces an increase in velocity fluctuations, and consequently an increase in turbulent kinetic energy. In compartment 1, in the vicinity of the inlet, a homogenization of the turbulent kinetic energy distribution is observed, strongly influenced by the turbulence input parameters such as the turbulent intensity. In this zone the lowest values of the turbulent kinetic energy are noted since air enters with a constant velocity so the fluctuations near the inlet are low which explains the low values of kinetic energy observed. The turbulent kinetic energy is higher in the flow area than in the vicinity of the walls. The forced convection of the air in the cavity intensifies the fluctuations of the velocities in this area and thus of the turbulent kinetic energy. In the vicinity of the walls, however, as the velocity distribution indicates, the velocities are low and therefore the kinetic energy.

The turbulent kinetic energy distribution is shown in Fig.7.a. It represents the kinetic energy of the velocity fluctuations. It can be seen that it is more important in the vicinity of the lower corners of the earth-to-air heat exchanger where the fluid starts to turn. Indeed, the presence of singular points of pressure drop in the configuration of the earth-to-air heat changer under study (in the U-shape) causes greater fluctuations in velocity at these points and consequently an increase in the turbulent kinetic energy. The velocity fluctuations continue in the middle of the main flow in the vertical outlet branch. This observation is explained by the increase in velocities due to the combined effects of natural and forced convection in the vertical direction, which induces an increase in velocity fluctuations, and consequently an increase in turbulent kinetic energy. In compartment 1, in the vicinity of the inlet, a homogenization of the turbulent kinetic energy distribution is observed, strongly influenced by the turbulence input parameters such as the turbulent intensity. In this zone the lowest values of the turbulent kinetic energy are noted since air enters with a constant velocity so the fluctuations near the inlet are low which explains the low values of kinetic energy observed. The turbulent kinetic energy is higher in the flow area than in the vicinity of the walls. The forced convection of the air in the cavity intensifies the fluctuations of the velocities in this area and thus of the turbulent kinetic energy. In the vicinity of the walls, however, as the velocity distribution indicates, the velocities are low and therefore the kinetic energy.

Fig. 7b shows the isovaleurs of the turbulent kinetic energy dissipation rate. This turbulence parameter determines the amount of energy lost by viscous forces in the turbulent flow. The analysis of Fig. 7.b shows that the distribution of the turbulent kinetic energy dissipation rate is homogeneous throughout the cavity and has low values except in the vicinity of the walls where the viscous forces are more intense.

The turbulent viscosity distribution is given in Fig. 7.c. It describes the dissipation of the turbulent kinetic energy. Its distribution in the earth-to-air heat exchanger is similar to that of the turbulent kinetic energy. The high values are observed at the vertical branches of the earth-to-air heat exchanger and at the elbows, while a uniform distribution is observed in the vicinity of the inlet and the walls of the earth-to-air heat exchanger. The low values indicate a lesser effect of viscous forces, while the high values indicate a greater influence of viscous forces. These results are consistent with the distribution of the turbulent kinetic energy (Fig. 7.a) and its dissipation rate (Fig. 7.b).

The distributions of the turbulence intensity, which represents an indicator of the turbulent agitation with respect to the mean kinetic energy field are similar to those described by the turbulent kinetic energy (Fig. 7a) and the turbulent viscosity (Fig. 7c). Thus, the turbulence intensity is characterized by maximum values at the core of the main flow, at the bends (area where the flow changes direction) and in the vicinity of the outlet. The minimum values of the turbulent intensity are located in the vicinity of the walls and especially at the entrance of the channel, thus showing the decrease of the turbulence intensity. These observations are consistent with the analyses made previously for the distributions of the turbulent kinetic energy (Fig. 7.a) and the turbulent viscosity (Fig. 7c).

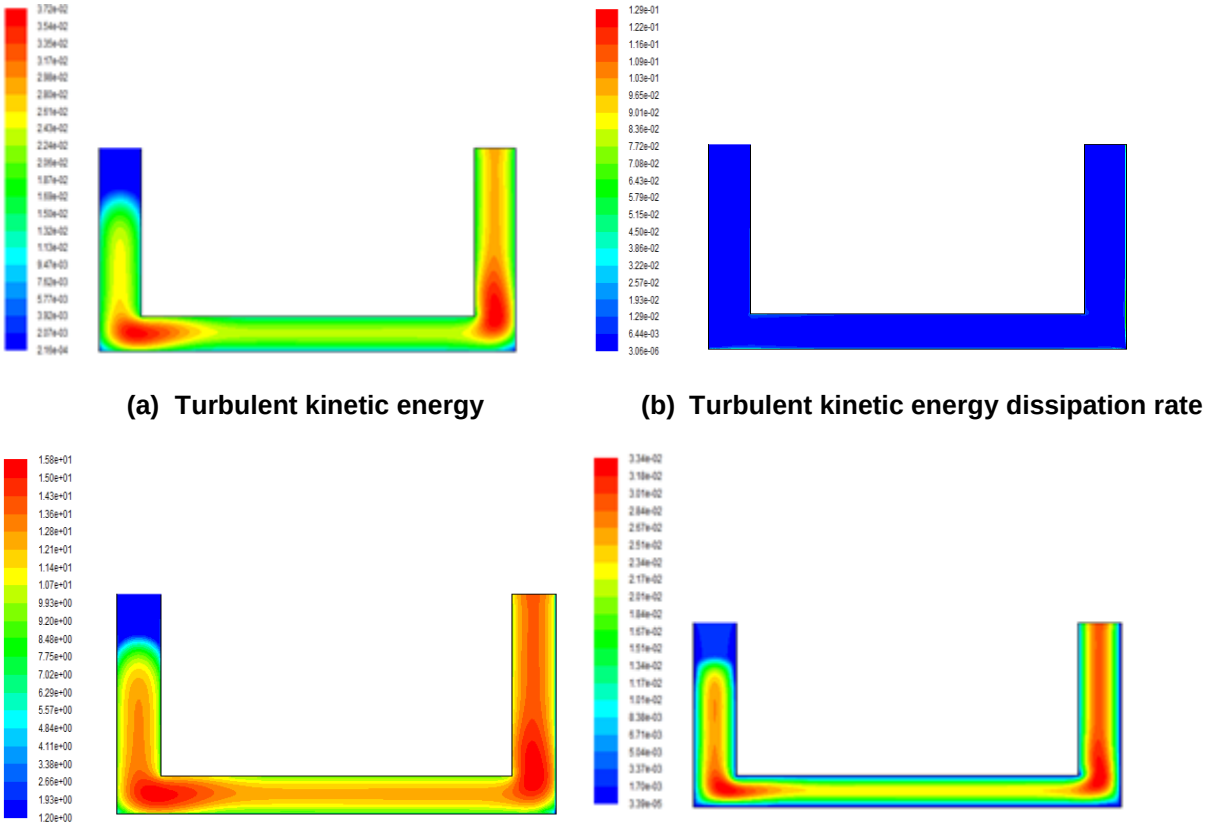

(a) Turbulent kinetic energy **(b) Turbulent kinetic energy dissipation rate**

(c) Turbulent viscosity **(d) Turbulence intensity**

Fig. 7. Turbulence parameters distribution for Re=10000

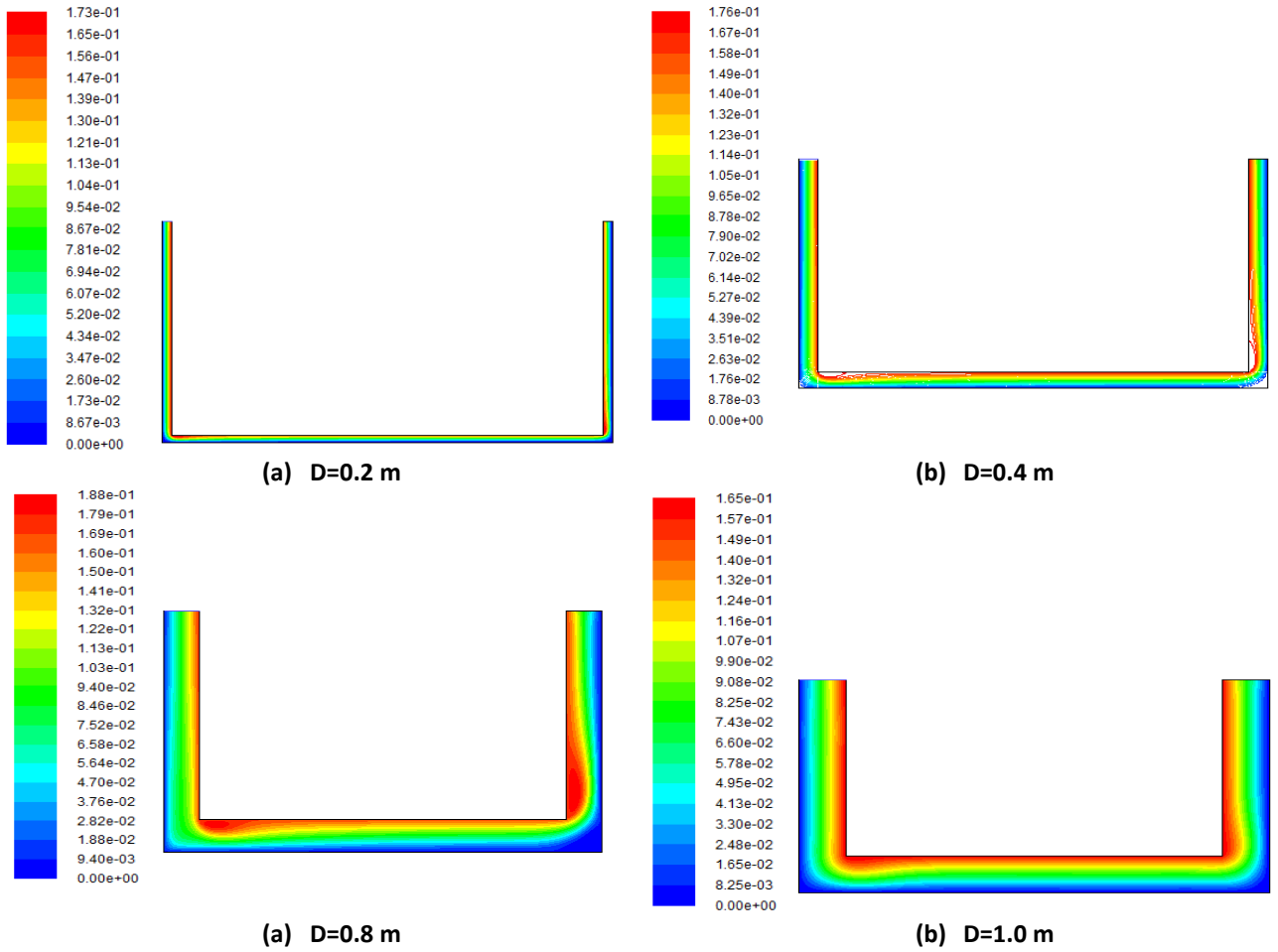

Fig. 8. Streamlines distribution for L=10 m, Re=25000, sandy soil. Effect of the diameters of the earth-to-air heat exchanger

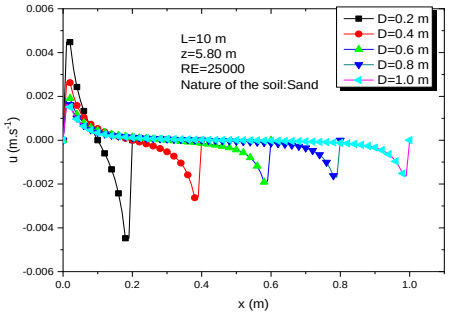
L=10 m
z=5.80 m
RE=25000
Nature of the soil:Sand
D=0.2 m
D=0.4 m
D=0.6 m
D=0.8 m
D=1.0 m
u (m.s-1)
x (m)

(a)

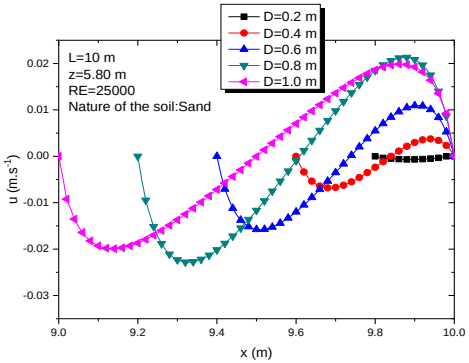
L=10 m
z=5.80 m
RE=25000
Nature of the soil:Sand
D=0.2 m
D=0.4 m
D=0.6 m
D=0.8 m
D=1.0 m
u (m.s-1)
x (m)

(c)

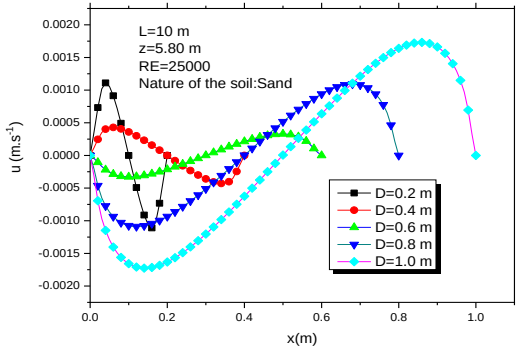
L=10 m
z=5.80 m
RE=25000
Nature of the soil:Sand
D=0.2 m
D=0.4 m
D=0.6 m
D=0.8 m
D=1.0 m
u (m.s-1)
x(m)

(b)

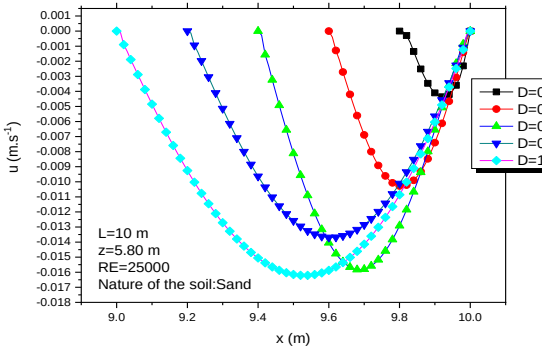
L=10 m
z=5.80 m
RE=25000
Nature of the soil:Sand
u (m.s-1)
x (m)

(d)

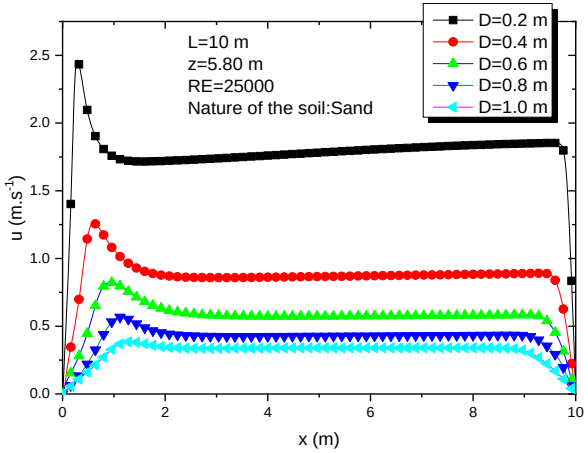

(e)

Fig. 9. Profile of the u component of the velocity versus x 0. Effect of the diameter of the earth-to-air heat exchanger

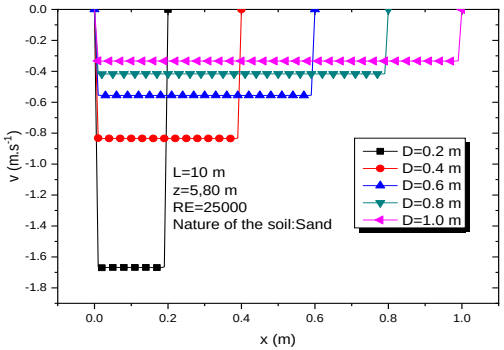

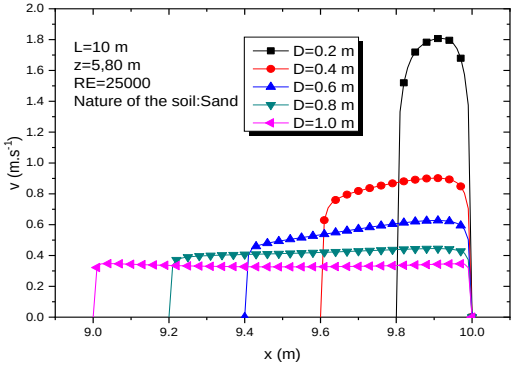

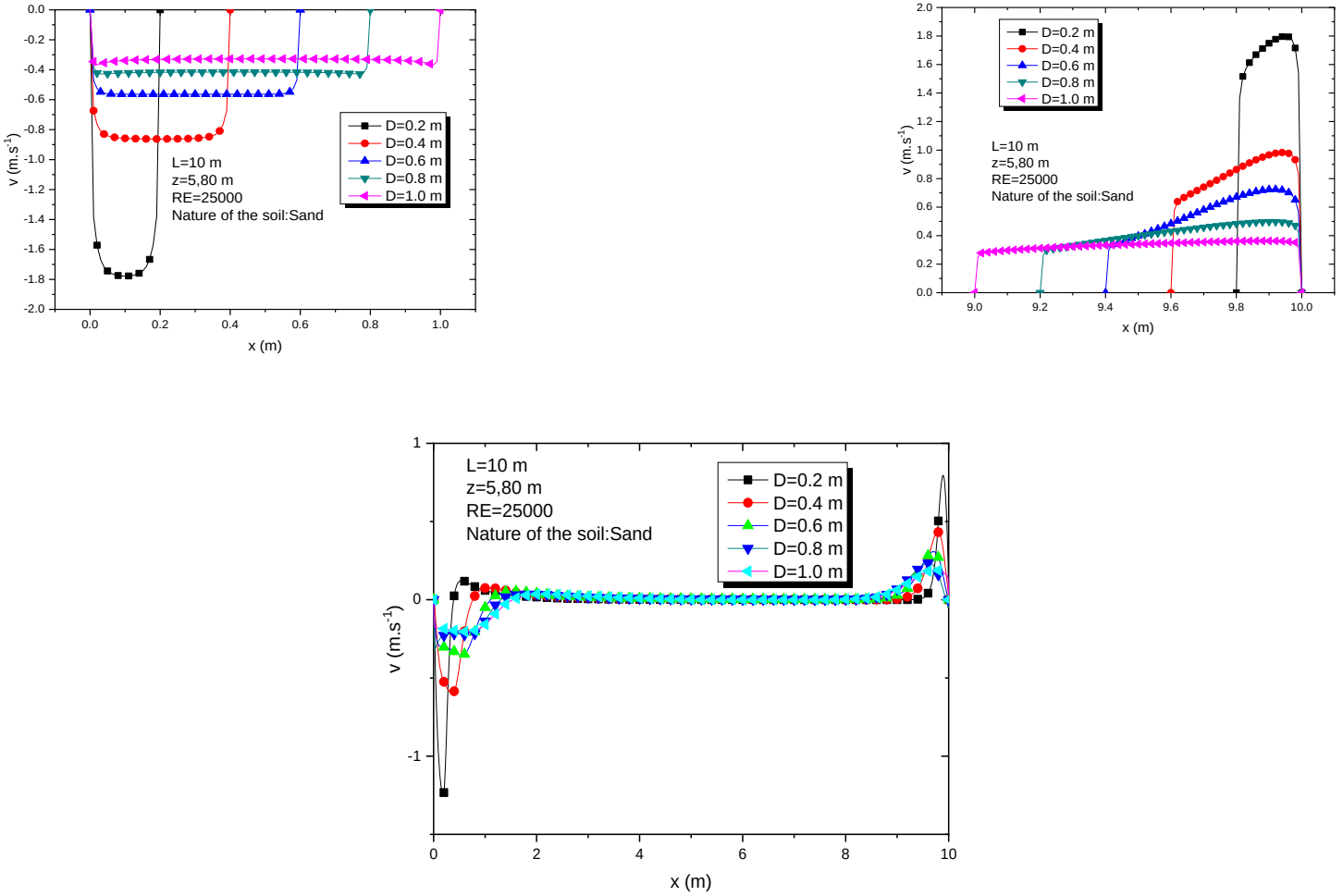

Fig. 10. Profile of the v component of the velocity versus x. Effect of the diameter of the earth-to-air heat exchanger

4.3 Study of the Influence of the Operating Parameters on the Potential Cooling of the Earth-to-air Heat Exchanger

4.3.1 Effects of the diameter on flow structure and temperature field

4.3.1.1 Flow structure

Fig. 8 shows the influence of the diameter of the earth-to-air heat exchanger on the flow. In order to analyze the effect of the variation of the diameter on the flow structure, it is chosen different values of the diameter: 0.2 m, 0.4 m, 0.8 m and 1.0 m. It can be seen that the variation of the diameter does not influence the distribution of the streamlines in a significant way. However, we note an increase in the values of the stream function as the diameter increases. But for a larger diameter (D=1.0 m), a decrease of the stream function value was observed. This shows that the choice of the diameter can influence the intensity of the forced convection in the channel.

Fig. 9 shows the profile of the horizontal component of the velocity as a function of x for different values of the diameter in several sections of the exchanger. It can be seen that the variation of the diameter has a considerable influence on the velocities profiles in the different compartments of the earth-to-air heat exchanger. Fig. 9.a shows that near the inlet the profiles of the horizontal component of the velocity (u) are similar for different values of the diameter. But the values of the amplitudes of u decrease as the diameter increases. In the same compartment for a lower section, the velocity profiles and their amplitudes change with diameter (Fig. 9.b). The u component undergoes a random variation in this section for different values of the diameter. In compartment 3, the variation in diameter shows that the velocity profile is not modified when the diameter is varied in each section of the compartment. However, from one section to another a difference in the u-profile can be observed. Analysis of Fig. 9.c and reveals that the values of the amplitude of the horizontal component of the velocity increase with diameter. The change in sign of the u component of velocity observed in compartments 1 and 3 shows that the fluid sometimes flows towards the left or right wall of compartment 1 and 3. This result is consistent with the observation made at the streamlines where a flow laminating the walls of the earth-to-air heat exchanger is observed. The horizontal component of the velocity in compartment 2 keeps the same profile and positive sign (Fig. 9.e) for different diameters of the earth-to-air heat exchanger. This indicates that the flow of air leaves compartment 1 to compartment 2 and with a velocity whose magnitude is proportional to the diameter as observed in compartment 3.

For more details on the flow structure, it is represented in Fig. 10, the vertical velocity profiles for different values of the depth of the earth-to-air heat exchanger and for different sections. In contrast to the horizontal component of the velocity (u), it can see that the vertical component of the velocity keeps the same shape and sign in the vertical parts of the exchanger. In compartment 1, the negative sign of v indicates that the flow is from top to bottom, while in compartment 3, the positive sign means that the air flow is from bottom to top. It can also be seen that the magnitude of the component decreases as the diameter increases. In compartment 2, the velocity component v is zero except in the vicinity of the left and right vertical walls. The spatial distribution of v and u corroborates and indicates that the flow is from compartment 1, goes through compartment 2 to compartment 3. This is consistent with the observed streamline distribution.

4.3.1.2 Temperature field

Fig. 11 shows the distribution of isotherms in the U-shaped tube of earth-to-air heat exchanger for different values of diameters. An analysis of this figure shows that the isotherm distributions are similar for the different diameters considered. However, the thermal field increases as the diameter increases. The minimum and maximum temperature values remain the same regardless of the diameter.

To support the observations made on the isotherm distribution, a more detailed analysis is made of the temperature profiles as a function of x, at different levels in the earth-to-air heat exchanger and for different diameters (Fig. 12). It can be seen that the temperatures keep the same profile for the different diameters. In the air inlet compartment the temperature amplitudes in a section are the same when the diameter varies. For the horizontal part of the system and in the outlet compartment the temperatures have the same pattern for all diameters. However, the temperature amplitude increases as the diameter increases. The diameter of the pipe defines the total section through which the air will circulate. It

influences both the air flow speed and the contact surface between the air and the ground. As the diameter of the pipe increases, the outlet temperature increases as shown in Fig. 12.c resulting in a reduction in the heat transfer coefficient at the inner surface of the pipe. As a result the cooling potential of the earth-to-air heat exchanger decreases as the diameter increases.

Fig. 4 shows the distribution of isotherms in the "U" shaped air/soil exchanger for different values of the diameters. An analysis of this figure showed that the isotherm distributions are similar for the different diameters considered. However, the thermal field increases as the diameter increases. The minimum and maximum values of the temperatures remain identical whatever the diameter.

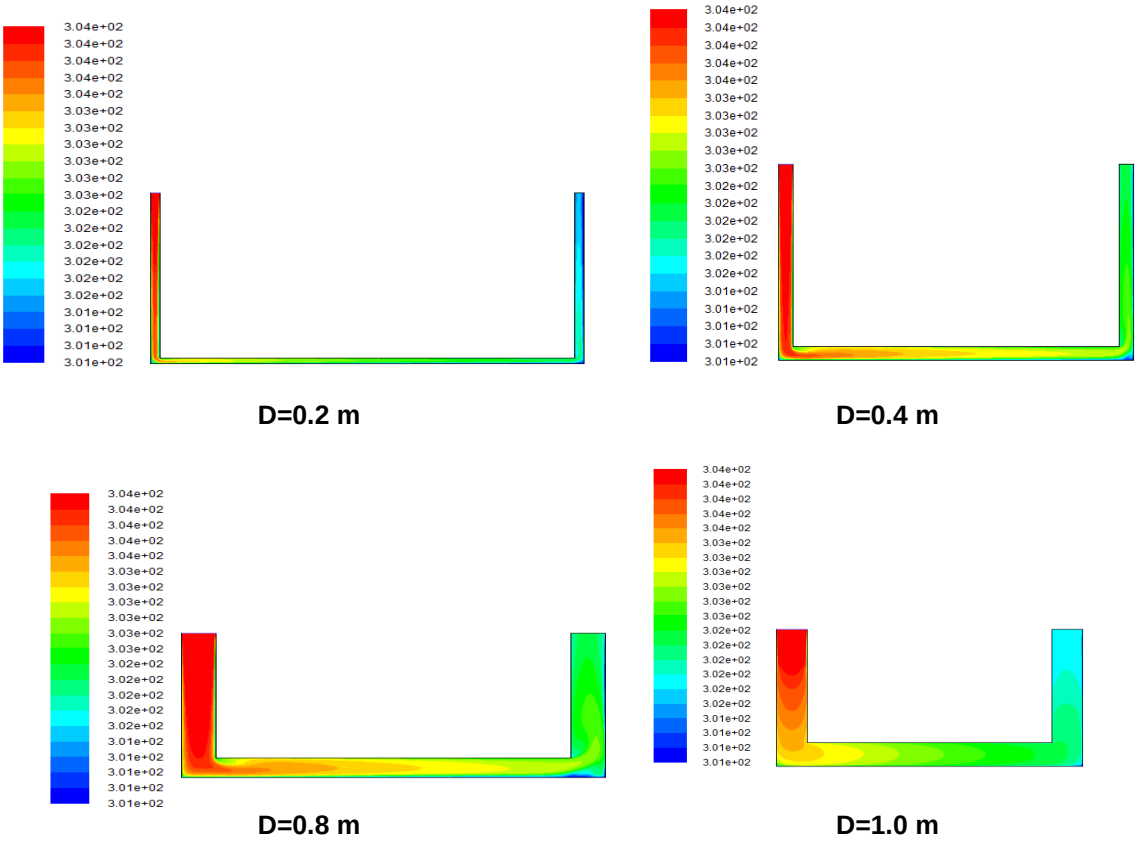

Fig. 11. Distribution of isotherms for L=10 m, Re=25000, sandy. Effects of the diameter of the earth-to-air heat exchanger

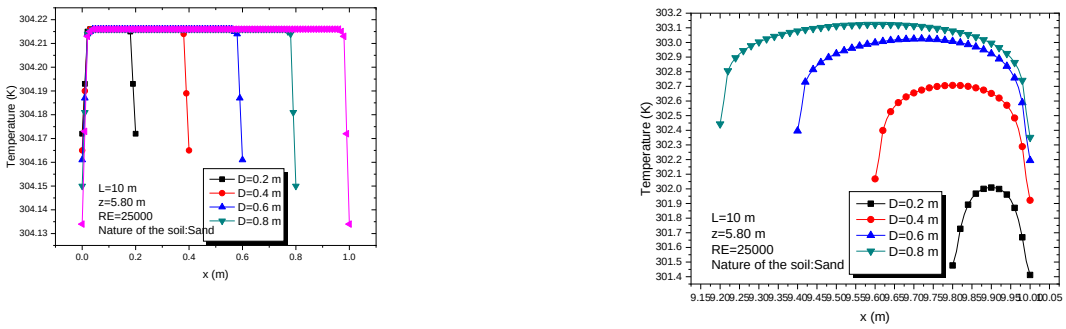

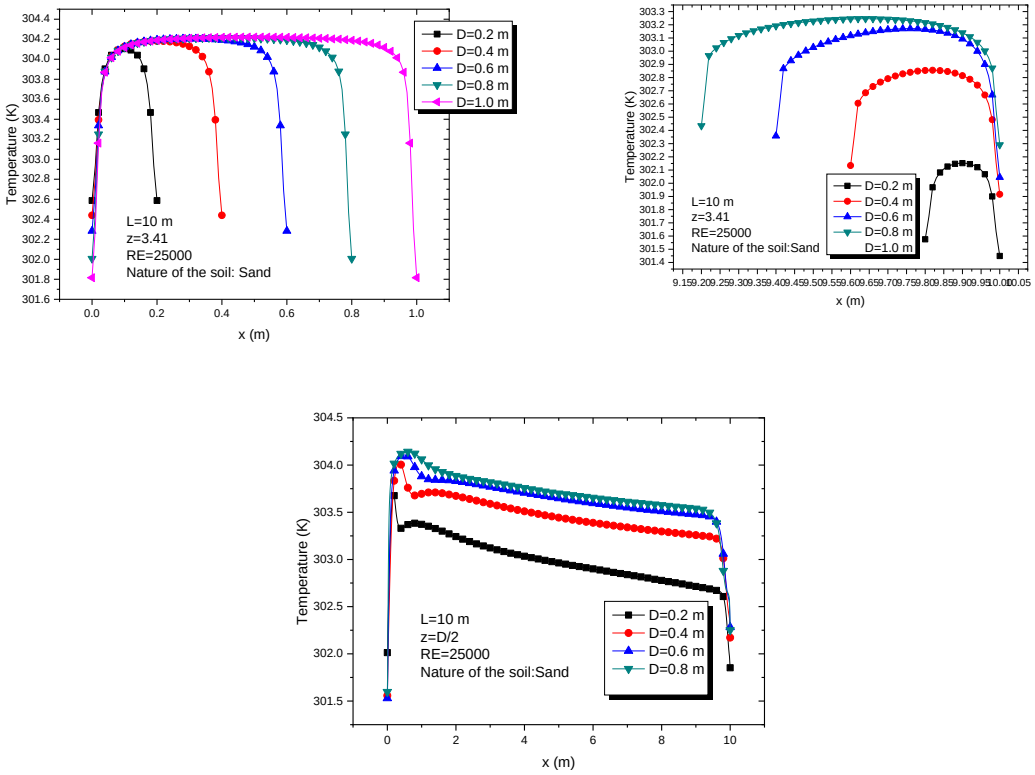

Fig.12. Temperature profile versus x. Effect of the earth-to-air heat exchanger diameter

The analysis of the profiles shows that the temperatures keep the same pattern for the different diameters. In the air inlet compartment the temperature amplitudes in one section are the same when the diameter varies. For the horizontal part of the exchanger and in the outlet compartment the temperatures have the same trend for all diameters. However, the temperature amplitude increases when the diameter increases. Indeed, the diameter of the pipe defines the total section through which the air will circulate. It influences both the air flow speed and the contact surface between the air and the ground. As the diameter of the pipe increases, the outlet temperature increases resulting in a reduction of the heat transfer coefficient at the inner surface of the pipe. As a result, the cooling potential of the air/ground heat exchanger decreases as the diameter increases.

4.3.2 Effects of the length on flow structure and temperature field

4.3.2.1 Flow structure

In the study of the influence of length, in order to improve the readability of the spatial distribution of velocities, temperatures and turbulence parameters, a diameter of 1.0 m was considered.

Fig. 13 shows the flow structure in earth-to-air heat exchanger for different lengths. The distribution of the streamlines previously described is unchanged with the variation of the earth-to-air heat exchanger length. Only an increase in the length of the streamlines following the shape of the channel can be noticed.

Fig. 14 and Fig. 15 show the profiles of the horizontal (u) and vertical (v) components of the velocity versus x for different values of z, respectively. The analysis of these figures reveals a great similarity between the profiles. The variation of the length has very little influence on the profiles of the horizontal and vertical components. The only noticeable deviation is in the middle of the inlet and outlet compartments for the u-component due to the higher convective exchange in these areas.

The highest values of u are located near the vertical walls, and the lowest values are found in the core of the main flow in compartments 1 and 3 dominated by downward and upward airflow

respectively. However, the values of u are significant in the horizontal part of the earth-to-air heat exchanger because in this area the flow is mainly along the horizontal axis driven by the u component. The opposite is observed for the v component, whose negative value indicates a descent of the air in the channel and whose positive value indicates an ascent of the air towards the earth-to-air heat exchanger outlet.

4.3.2.2 Temperature field

The thermal field (Fig. 16) shows that the heat exchange between the walls and the ventilation air is limited in the left vertical column. Indeed, the still high ventilation speed (thus a high flow rate) does not favor a fast heat transfer. In the rest of the channel, the fluid is practically isothermal at the same temperature as the walls.

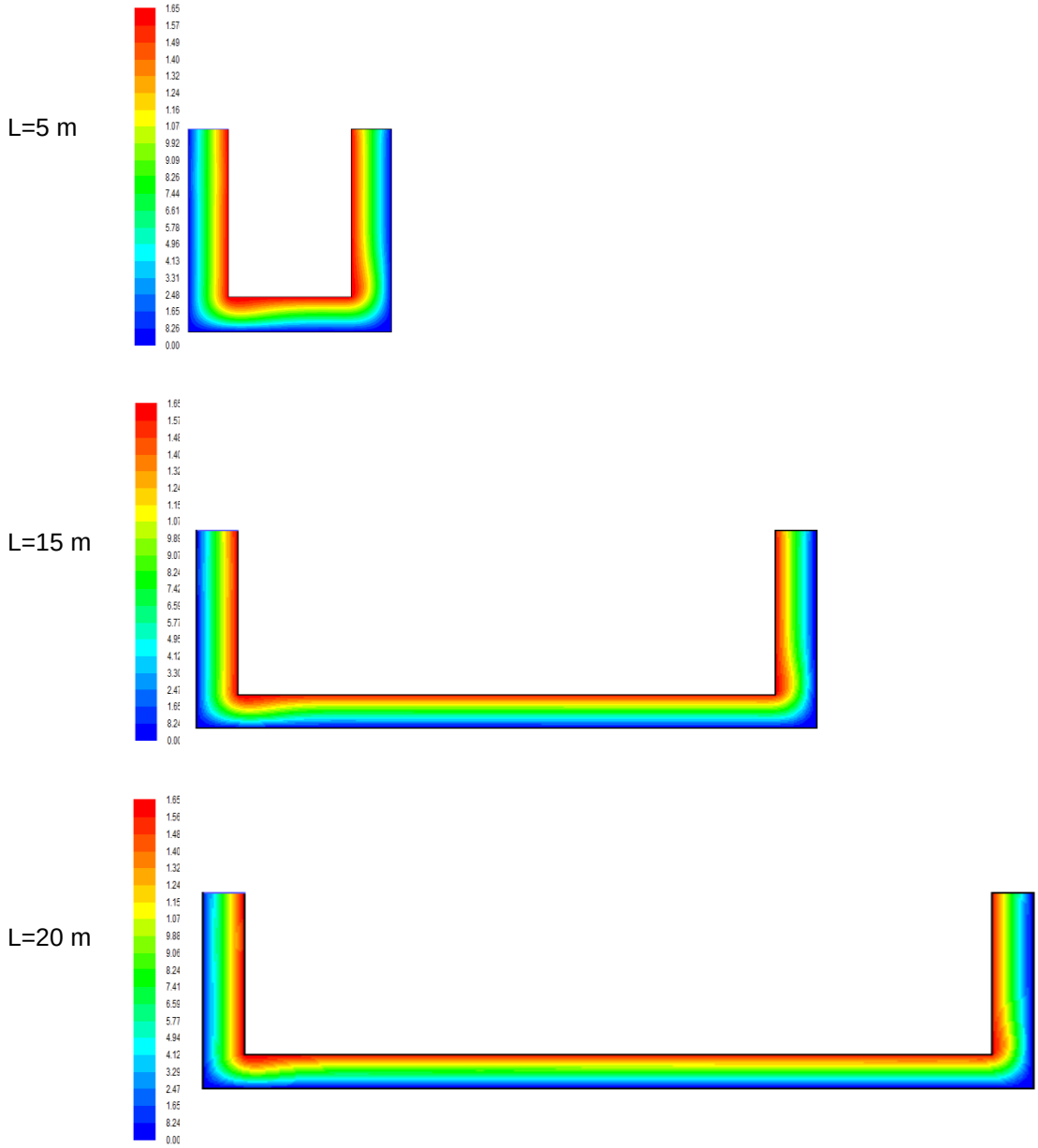

Fig. 13. Distribution of streamlines for different lengths

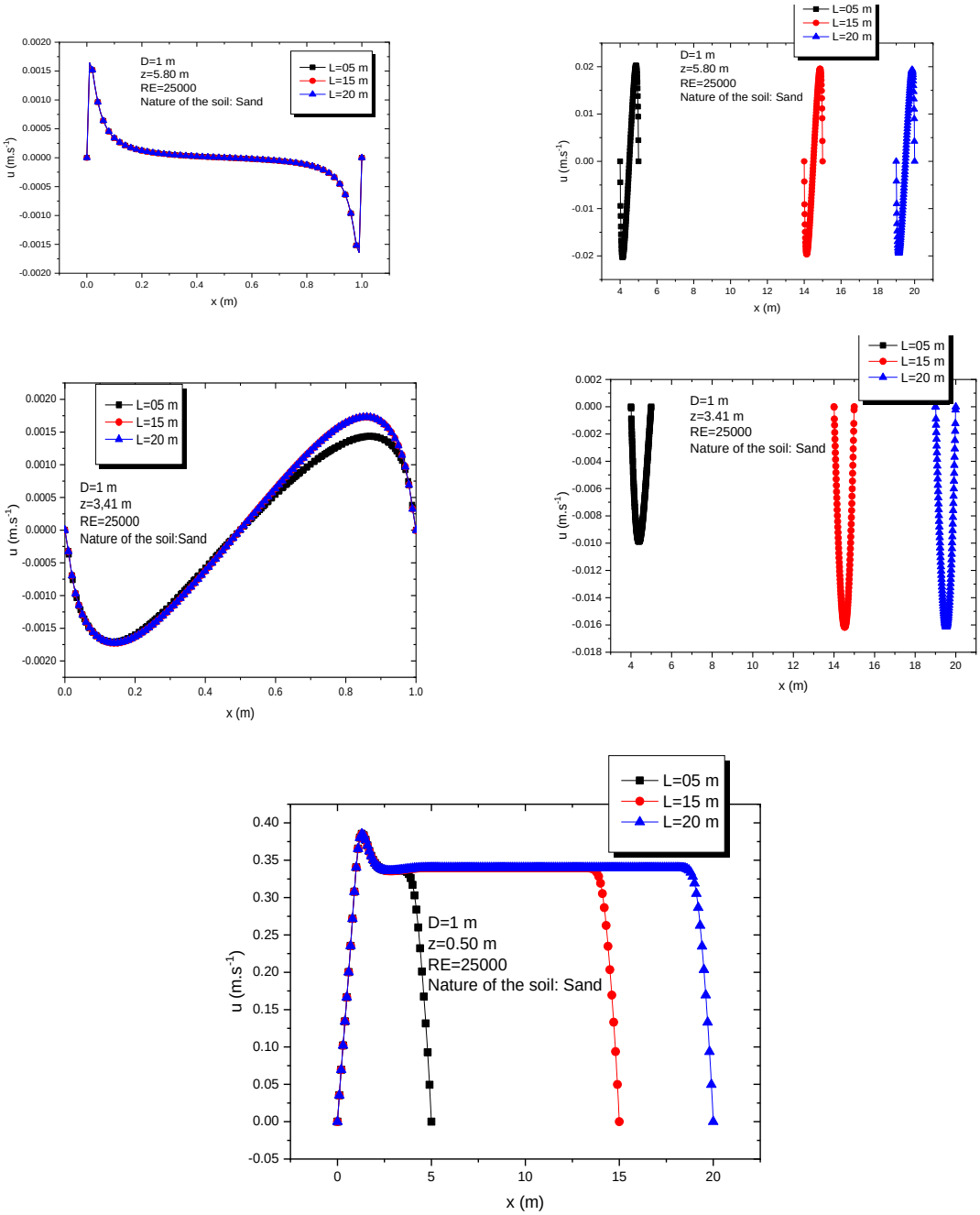

Fig. 14. Profile of the u component of the velocity versus x. Effect of the lenth of the earth-to-air heat exchanger

The influence of the length on the temperature distribution is shown in Fig. 16. As the length of the heat exchanger is increased, the isotherms increase as a result of the intensification of heat exchange between the walls and the convective jet. The temperature in the air outlet compartment is lower as the length of the earth-to-air exchanger increases. Indeed, the increase in length leads to an increase in the heat exchange surface between the air and the walls of the earth-to-air heat exchanger in thermal equilibrium with the ground. As the temperature of the ground is lower than that of the ambient air, the air cools better when the length is greater.

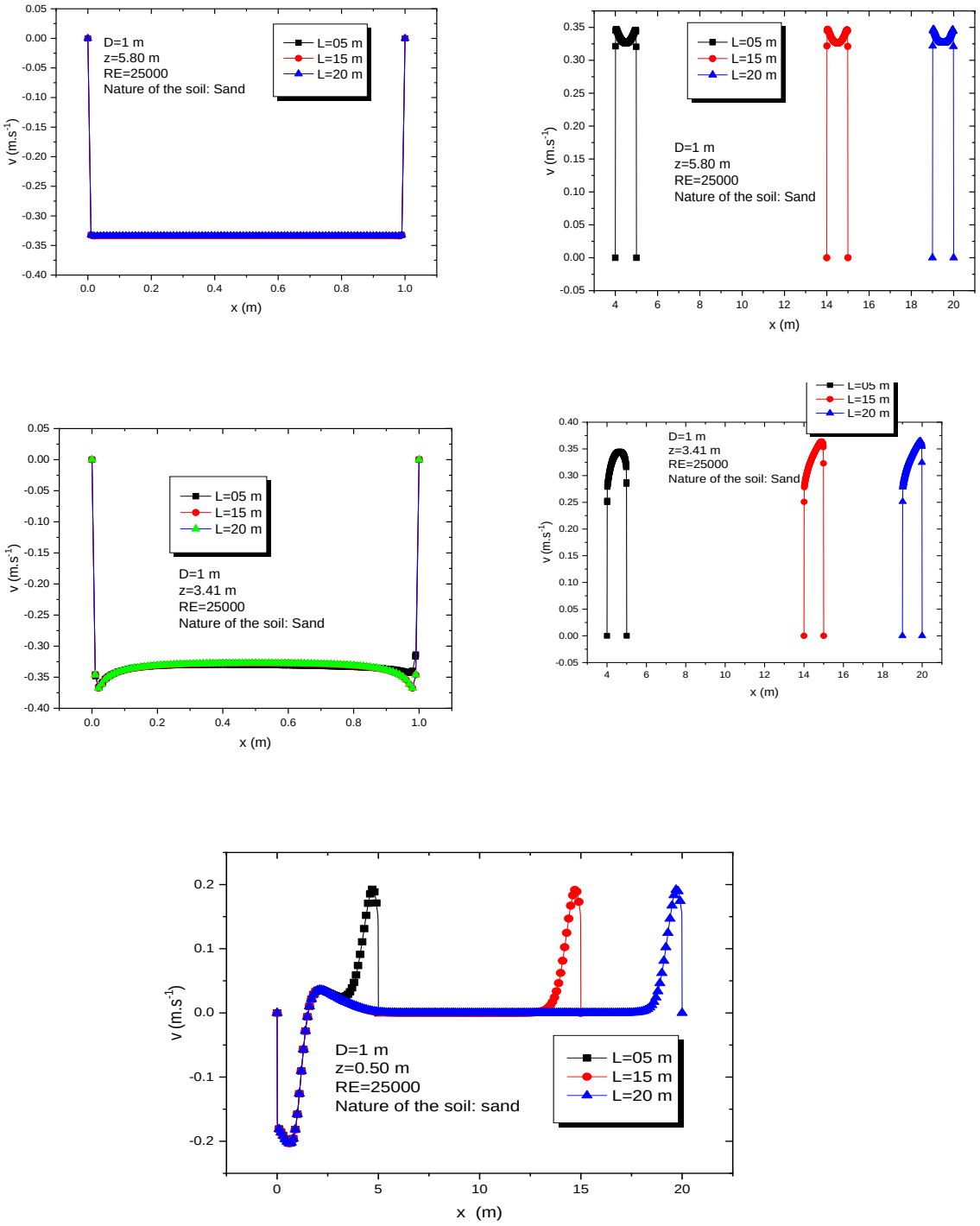

Fig. 15. Profile of the v component of the velocity versus x. Effect of the lenth of the earth-to-air heat exchanger

In order to better understand the influence of the length on the thermal field, the temperature profiles as a function of the abscissa x in several sections of the earth-to-air heat exchanger under the influence of the length variation are presented in Fig. 17. The analysis of this figure shows that in compartment 1, the temperature profiles as a function of x are identical. The

reason for this is that in this area the air velocity is higher, so the heat exchange between the air and the walls of the earth-to-air heat exchanger at ground temperature is limited. The evolution of the flow in the horizontal part of the earth-to-air exchanger, where the exchange surface increases with the length, leads to a significant decrease in the temperature value (Fig. 17.e) with the length. The same observation can be made in the outlet compartment. In this compartment the temperature near the outlet decreases progressively as the length increases.

Further analysis (Fig. 18) of the influence of the length shows that there is a threshold length of about 40 m from which the increase of the length of the earth-to-airheat exchanger does not influence the temperature of the air at the outlet any more. According to this result, it is considered that the variation of the channel length in the range of 5 m≤L≤40 m is sufficient to obtain a better heat exchange in this kind of configuration and consequently a good cooling of the air using the earth-to-air heat exchanger.l.

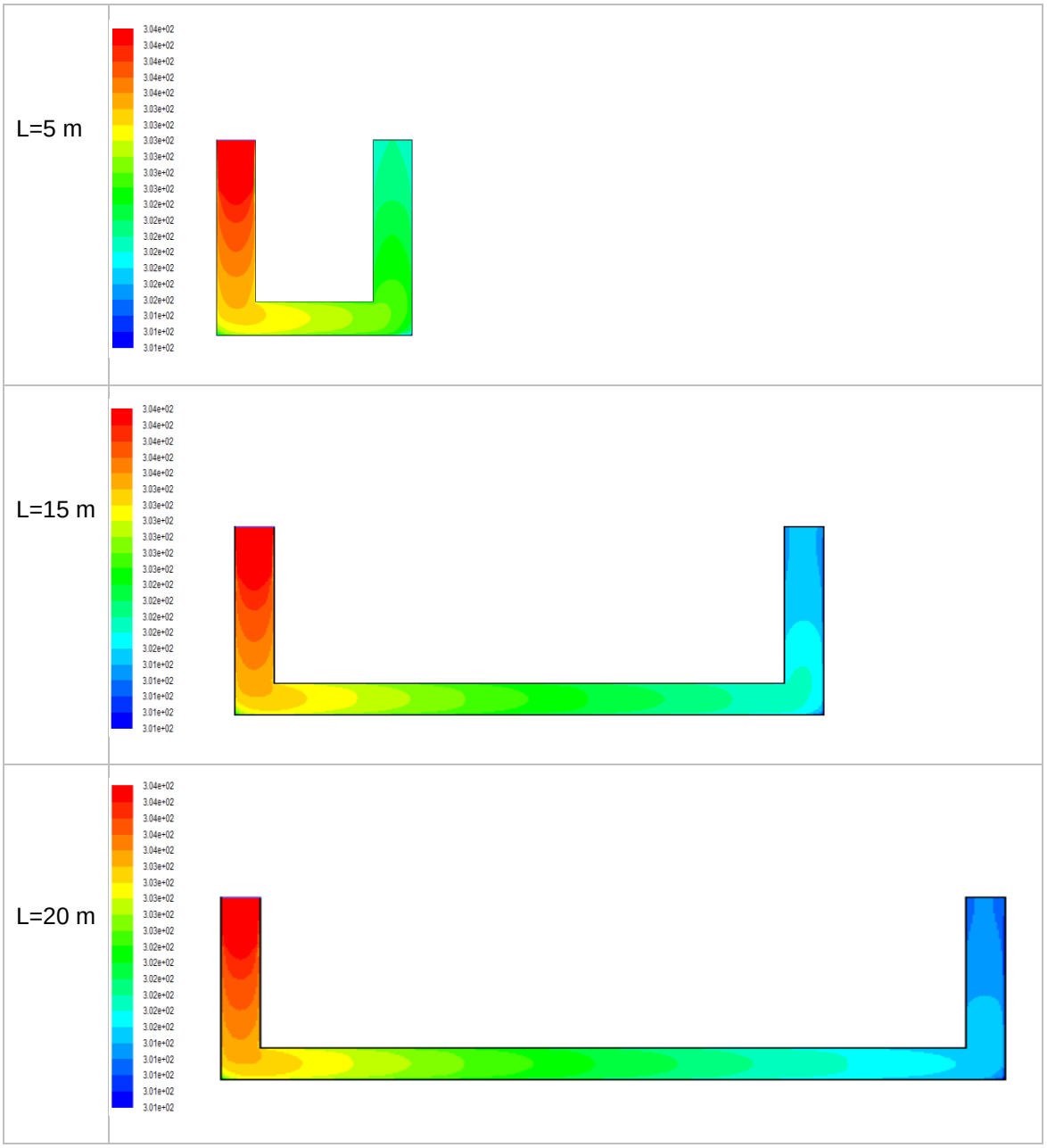

Fig. 16. Distribution of isotherms for different lengths

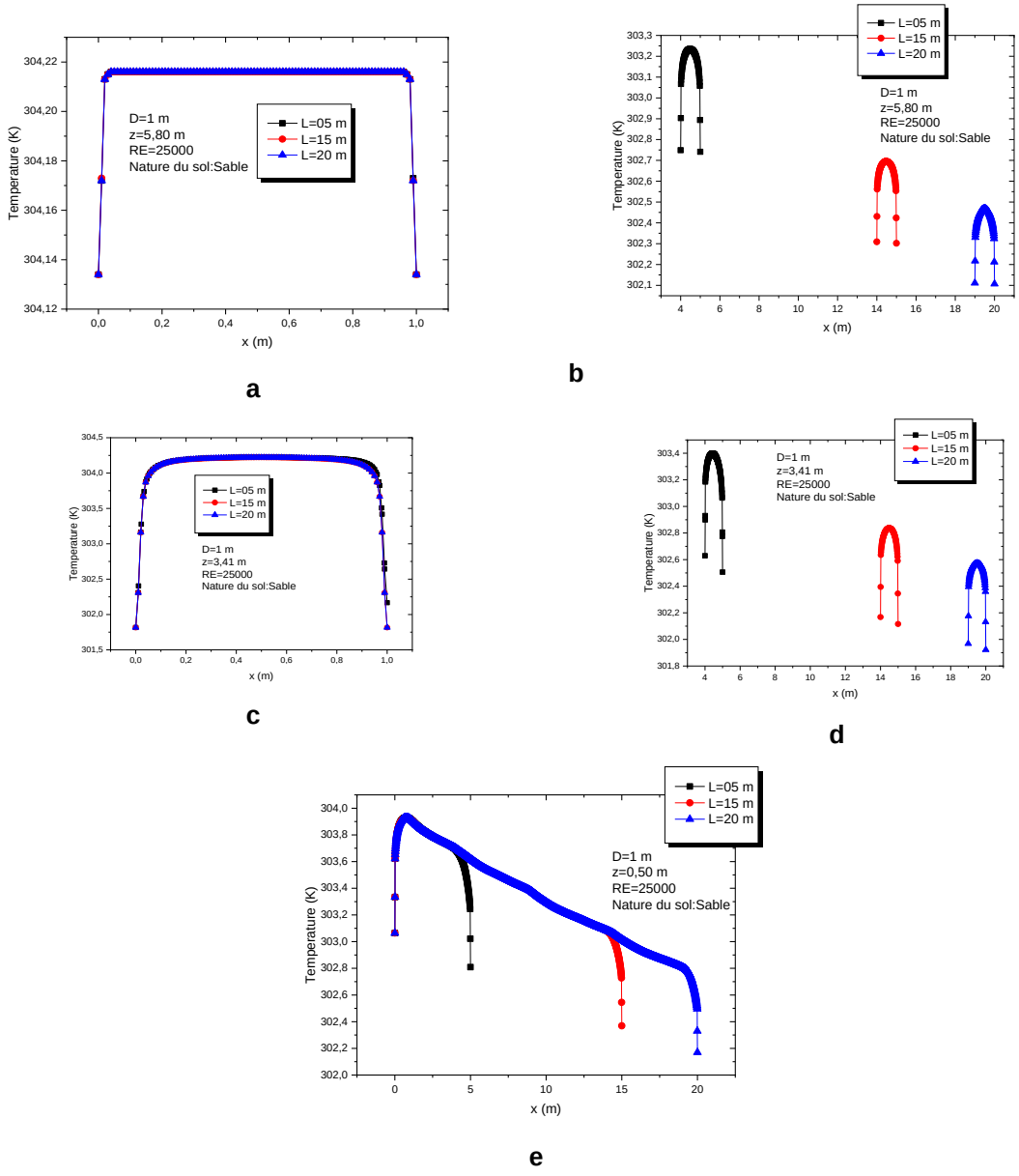

Fig. 17. Temperature profile versus x. Effect of the earth-to-air heat exchanger lenth

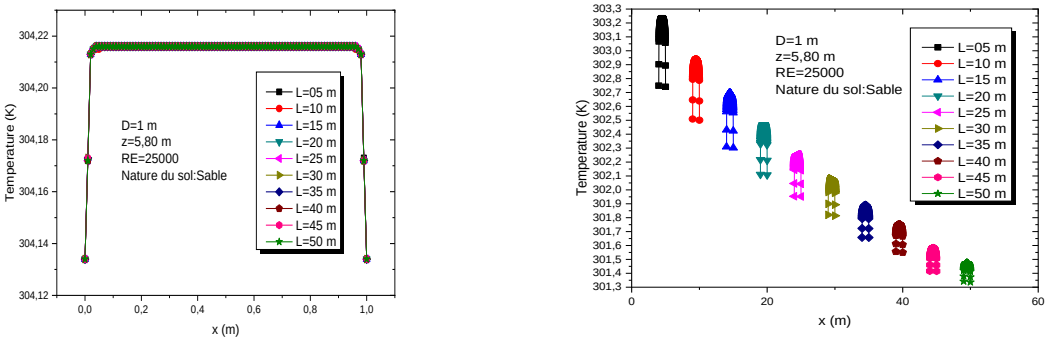

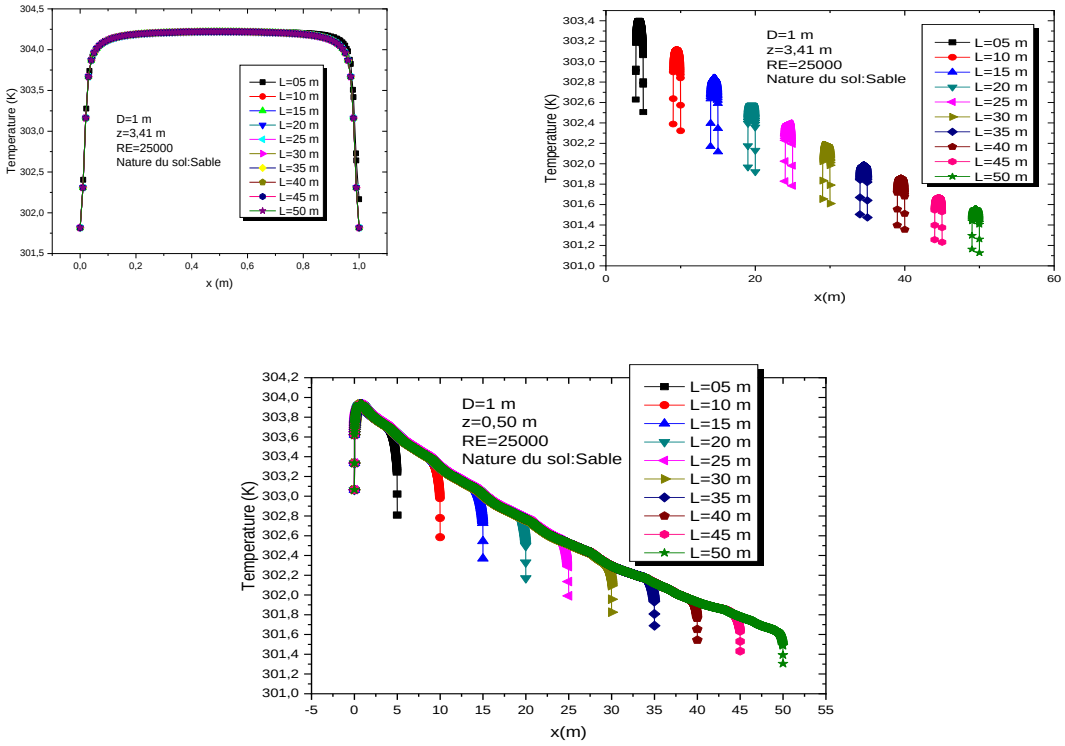

Fig. 18. Temperature profile versus x. Optimal earth-to-air heat exchanger lenth for room cooling

5. CONCLUSION

This work is devoted to the numerical study of the earth-to-air heat exchanger in turbulent regime air flow. The Navier-Stokes equations and heat transfer equation associated to $k-\varepsilon$ model for turbulence are presented. The transfer equations and the associated initial and boundary conditions were discretized using finite volume method. The proposed model was validated against experimental data and numerical study and was found to accurately predict the temperature of the circulated air and the temperature distribution in earth-to-air heat exchanger, as well as the overall thermal performance of the earth-to-air heat exchangers The numerical results were presented in terms of streamlines, isotherms and profiles of velocity and temperature. The effects of the diameter and the length of the earth-to-air heat exchanger on the flow structure and temperature field are investigated. The outcomes of this study is given follow:

- The flow structure is characterized by open streamlines that are parallel to each other and to the walls of the earth-to-air heat exchanger indicating that the heat transfers are mainly dominated by forced convection.
- The isotherms are made up of a succession of parabolic shaped cells originating at the inlet of the exchanger and following the shape of the channel.
- The variation of the diameter does not influence the distribution of the streamlines in a significant way. However, the values of the stream function increases when the diameter increases
- The distribution of the streamlines previously described is unchanged with the variation of the earth-to-air heat exchanger length. Only an increase in the length of the streamlines following the shape of the channel can be noticed.
- The isotherm distributions are similar for the different diameters considered. However, the thermal field increases as the diameter increases. The minimum and maximum temperature values remain the same regardless of the diameter.
- When diameter of the pipe increases, the outlet temperature increases resulting in a

reduction in the heat transfer coefficient at the inner surface of the pipe.

- The increase of the length of the earth-to-air heat exchanger, the isotherms increase as a result of the intensification of heat exchange between the walls and the convective jet. The temperature in the air outlet compartment is lower as the length of the earth-to-air exchanger increases.

ACKNOWLEDGEMENT

The authors thank the Director and staff members of National Metrological Ser-vice of National Aviation Security Agency (ASECNA) of Togo for providing climate data required for this work. They are also grateful to the anonymous reviewers for their thorough reviews, helpful comments and suggestions.

COMPETING INTERESTS

Authors have declared that no competing interests exist.

REFERENCES

1. Antinucci M. Fleury B, Lopez d' Asiain J, Maldonado E, Santamomis M, Tombazis A, Yannas S. Passive and hybrid cooling of buildings-state of the art. Int. J. Solar Energy. 1992;11:251-272.
2. Santamouris M, Argiriou A, Vallindras M. Design and operation of a low energy consumption passive solar agricultural greenhouse. Solar Energy. 1994;52(5). DOI:https://doi.org/10.1016/0038-092X(94)90114-H
3. Bisoniya TS., Kumar A. Baredar P. Experimental and analytical studies of earth-air heat exchanger (EAHE) systems in India: a review. Renewable and Sustainable Energy Reviews. 2013;19:238–246. DOI:https://doi.org/10.1016/j.rser.2012.11.023
4. Lund JW, Freeston DH, Boyd TL. Direct application of geothermal energy: worldwide review. Geothermics. 2005;34(6):691-727 DOI:https://doi.org/10.1016/j.geothermics.2005.09.003
5. Bisoniya TS. Design of earth–air heat exchanger system. Geothermal Energy. 2015;3(1):1-0. DOI:https://DOI10.1186/s40517-015-0036-2
6. Santamouris M, Pavlou K, Synnefa A, Niachou K, and Kolokotsa D. Recent progress on passive cooling techniques. Advanced technological developments to improve survivability levels in lowincome households. Energy and Building. 2007; 39(7):859-866. DOI:https://doi.org/10.1016/j.enbuild.2007.02.008
7. Santamouris M, Gaitani N, Spanou A, Saliari M, Giannopoulou K et al. Using cool paving materials to improve microclimate of urban areas - Design realization and results of the flisvos project. Building and Environment. 2012;53: 28–136. DOI:https://doi.org/10.1016/j.buildenv.2012.01.022
8. Santamouris M, Synnefa A, Karlessi T. Using advanced cool materials in the urban built environment to mitigate heat islands and improve thermal comfort conditions. Solar Energy. 2011;85(12): 3085–3102. DOI:https://doi.org/10.1016/j.solener.2010.12.023
9. Bisoniya TS, Kumar A, Baredar P. Experimental and analytical studies of earth– air heat exchanger (EAHE) systems in India: a review. Renewable and Sustainable Energy Reviews. 2013;19:238–46. DOI:https://doi.org/10.1016/j.rser.2012.11.023
10. Ozgener O, Ozgener L. Determining the optimal design of a closed loop earth to air heat exchanger for greenhouse heating by using exergoeconomics. Energy and Buildings. 2011;43(4):960-965. DOI:https://doi.org/10.1016/j.enbuild.2010.12.020
11. Florides G, Kalogirou S. Ground heat exchangers-a review of systems, models and application. Renewable Energy. 2007;32(15):2461–78. DOI:https://doi.org/10.1016/j.renene.2006.12.014
12. Vaz J, Sattler MA, dos Santos ED, Isoldi LA. Experimental and numerical analysis of an earth–air heat exchanger. Energy and Building. 2011;43(9):2476–2482. DOI:https://doi:10.1016/j.enbuild.2011.06.003
13. Li H, Yu Y, Niu F, Michel S, Chen B. Performance of a coupled cooling system with earth-to-air heat exchanger and solar chimney. Renewable Energy. 2014;62:468–477.

DOI:https://doi.org/10.1016/j.renene.2013.08.008

14. Selamat S, Miyara A, Kariya K. Numerical study of horizontal ground heat exchangers for design optimization. Renew. Energy. 2016;95:561–573. DOI:https://doi.org/10.1016/j.renene.2016.04.042
15. Sodha MS, Mahajan U, Sawhney RL. Thermal performance of a parallel earth air-pipes system. Int. J. Energy Res. 1994;18:437-447. DOI:https://doi.org/10.1002/er.4440180404
16. Thiers S. Bilans Energétiques et Environnementaux de Bâtiments à Energie Positive. PhD thesis, Ecole Nationale Supérieure des Mines de Paris, November 2008.
17. De Paepe M, Janssens A. Thermo-hydraulic design of earth-air heat exchangers. Energy and Buildings. 2003;35(4):389-397. DOI:https://doi.org/10.1016/S0378-7788(02)00113-5
18. Badescu V, Sicre B. Renewable energy for passive house heating: II. Model. Energy and Buildings. 2003;35(11):1085–1096. DOI:https://doi.org/10.1016/S0378-7788(02)00113-5
19. Mathur A, Mathur S, Agrawal GD;Mathur J. Comparative study of straight and spiral earth air tunnel heat exchanger system operated in cooling and heating modes. Renewable Energy. 2017;108:474-487 DOI:https://doi.org/10.1016/j.renene.2017.03.001
20. Benrachi N, Ouzzane, M, Smaili A, Lamarche L, Badache M, Maref W. Numerical parametric study of a new earth-air heat exchanger configuration designed for hot and arid climates. Int. J. Green Energy. 2020;17:115–126. DOI:https://doi.org/10.1080/15435075.2019.1700121
21. Kanaris AG, Mouza AA, Paras SV. Flow and heat transfer predicition in a corrugated plate heat exchanger using a CFD code. Chemical Engineering & Technology. 2006;29(8):923-930. DOI:https://doi.org/10.1002/ceat.200600093
22. Wang Y, Dong Q, Liu M, Characteristic of fluid and heat transfer in shell side of heat exchangers with longitudinal flow of shell side fluid with different supporting structures. Proceedings of International Conference on Power Engineering. 2007; Hangzhou, China.
23. Kabashnikov VP, Danilevskii LN, Nekrasov VP and Vityaz IP. Analytical and numerical investigation of the characteristics of soil heat exchanger for ventilation systems. International Journal of Heat and Mass Transfer. 2002;45:2407-2418. DOI:https://doi.org/10.1016/S0017-9310(01)00319-2
24. Paepe MD, Janssens A. Thermo-hydraulic design of earth-air heat exchangers. Energy and Buildings. 2003;35(4):389-397. DOI:https://doi.org/10.1016/S0378-7788(02)00113-5
25. Zhou J, Wang H, Li X, Dai C. Experimental investigation and theoretical model of heat transfer of saturated soil around coaxial ground coupled heat exchanger. Applied Thermal Enginnering. 2008;28(2-3):116-125. DOI:https://doi.org/10.1016/j.applthermaleng.2007.03.033
26. Tittelein P, Achard G, Wurtz E. Modelling earth-to-air heat exchanger behaviour with the convolutive response factors method. Applied Energy. 2009;86(9):1638-1691. DOI:https://doi.org/10.1016/j.apenergy.2009.02.010
27. Ramırez L, Xaman JAJ, Alvarez G, Hernandez P. Numerical study of earthto-air heat exchanger for three different climates. Energy and Buildings. 2014; 76:238-248. DOI:https://doi.org/10.1016/j.enbuild.2014.02.073
28. Flaga M, Schnotale J, Radon J, Was K. Experimental measurements and CFD simulation of a ground source heat exchanger operating at a cold climate for a passive house ventilation system. Energy and Buildings. 2014;68:562-570. DOI:https://doi.org/10.1016/j.enbuild.2013.09.008
29. Cucumo M, Cucumo S, Montoro L, Vulcano. A dimension transient analytical model for earth-to-air-heat exchangers, taking into account condensation phenomena and thermal perturbation from the upper free surface as well as around the buried pipes. International of Heat and Mass Transfer. 2008;51(3-4):506-916. DOI:https://doi.org/10.1016/j.ijheatmasstransfer.2007.05.006
30. Sehli A, Hasni A, Tamali M. The potential of earth-air heat excahngers for low energy

cooling of buildings in South Algeria. Enegy Procedia. 2012;18:496-506. DOI:https://doi.org/10.1016/j.egypro.2012.05.061

31. Patankar SV. Numerical heat transfer and fluid flow. Hemisphere Publishing Corporation; 1980.
32. Patankar SV, Spalding DB. A calculation procedure for heat, mass and momentum transfer in three-dimensional parabolic flows. Int. J. Heat Mass Transf. 1972; 15(10)1787–1806. DOI:https://doi:10.1016/0017-9310(72)90054-3
33. Ampofo F, Karayiannis TG. Experimental benchmark data for turbulent natural convection in an air filled square cavity. Int. J. Heat Mass Transf. 2003;46(19)3551–3572. DOI:https://doi:10.1016/S0017-9310(03)00147-9.
34. Henkes RAWM, Hoogendoorn CJ. Comparison exercise for computations of turbulent natural convection in enclosures. Numer. Heat Transf. Part B Fundam. 1995. 28(1)59–78 DOI:https://doi:10.1080/10407799508928821

Peer-review history:
The peer review history for this paper can be accessed here:
https://www.sdiarticle5.com/review-history/95772